Title
ARCS: A one dimensional nonlinear soil model for ground response analysis

Authors
Yniesta, S
Brandenberg, SJ
Shafiee, A

Publication Date
2017-11-01

DOI
10.1016/j.soildyn.2017.08.015

Peer reviewed

ARCS: a One Dimensional Nonlinear Soil Model for Ground Response Analysis

Yniesta S.[a]*, Brandenberg S.J.[b], Shafiee A.[c]

[a]Department of Civil, Geological and Mining Engineering, Ecole Polytechnique de Montréal, 2900 Edouard Montpetit Blvd, Montreal, QC H3T 1J4 Canada

[b] Department of Civil and Environmental Engineering, University of California Los Angeles, 5732 Boelter Hall Box 951593 Los Angeles, CA 90095-1593, USA

[c] Group Delta Consultants Inc., 9245 Activity Rd #103, San Diego, CA 92126, USA

* corresponding author. *Tel.:* +1 514 817 4154 *E-mail Address:* samuel.yniesta@polymtl.ca

Abstract

This paper presents a one dimensional nonlinear stress-strain model called ARCS (Axis Rotation and Cubic Spline) capable of reproducing any user-input modulus reduction and damping curve. Unlike many previous nonlinear models, the ARCS model does not utilize Masing's rules, nor does it require a specific functional form for the backbone curve such as a hyperbola. Rather, the model matches the desired modulus reduction curve by fitting cubic splines to the implied stress-strain curve, and matches the damping curve by utilizing a coordinate transformation technique in which one axis lies along the secant shear modulus line with the other axis in the orthogonal direction for a particular unload-reload cycle. Damping is easily controlled in the transformed coordinate space. An inverse coordinate transformation returns the desired stress. The integration algorithm is independent of strain step size, meaning that the returned stress for a large strain increment is identical to the stress that would be returned by subdividing the strain increment into smaller increments. Small-strain damping may

be modeled hysteretically, avoiding the need for supplemental viscous damping. The model is shown to match the results of laboratory cyclic simple shear tests involving deliberately irregular stain histories. The performance of the model is illustrated in a set of ground response simulations where its predictions are compared with those of existing models. The ARCS model does not explicitly account for rate effects, cyclic degradation, or pore pressure generation. However, the equations can potentially be adapted in more advanced constitutive models to capture these effects. Such implementations are reserved for future publications.

1 Introduction

Earthquake ground motions are influenced by source, path, and site effects. Site effects are most commonly considered using either (1) nonlinear site amplification functions that depend on the average shear wave velocity in the upper 30m (V_{s30}), or (2) site-specific one-dimensional ground response analysis. Ground response analyses are performed using equivalent linear (EL) procedures, in which the shear modulus and damping are taken as time-invariant values set to be consistent with mobilized shear strains, or nonlinear (NL) procedures, in which nonlinear hysteretic unload/reload behavior is utilized to match desired modulus reduction and damping behavior. Recent studies indicate that NL procedures are superior to EL when mobilized shear strains exceed about 0.4% [1,2] or even as low as 0.05% [3]. These strain levels are exceeded at many sites where strong ground motions are imposed on soft soil profiles.

Nonlinear site response models focus on matching small-strain behavior measured in laboratory devices at shear strains lower than about 0.1 to 0.3%, but these models are often extrapolated beyond their range of experimental validation to larger strains. This extrapolation can cause an under- or over-prediction of shear strength depending on the ratio of shear strength to small strain shear modulus, G_{max}. These shear strength errors can translate to ground motion

prediction errors [4,5,6]. Developing models that accurately capture small strain behavior and shear strength is obviously important for nonlinear site response simulations.

This paper presents a one-dimensional nonlinear stress-strain model called ARCS (Axis Rotation and Cubic Spline) capable of reproducing any user-input modulus reduction and damping curve. Existing models commonly used in site response modeling are discussed first to illustrate the need for improved models. This is followed by presentation of the proposed modeling equations, which are shown to precisely match any user-input modulus reduction and damping curve. The ARCS model is then compared with direct simple shear laboratory experiments conducted on sand and peat soils to illustrate key features of behavior and compare with existing model formulations. Lastly, the model has been implemented in DEEPSOIL using the recently developed user-defined model, and the performance of the model is illustrated through a set of ground response simulations on a simple profile, and the results are compared with those obtained with existing models.

2 Modulus Reduction Behavior of Existing Models

User inputs to a one-dimensional ground response analysis for each soil layer include: (1) maximum shear modulus, (2) modulus reduction curve, and (3) damping ratio curve. Existing nonlinear models vary in their ability to capture the desired modulus reduction and damping behavior. Models are categorized as either one-dimensional, consisting of a backbone curve and unload-reload relations, or multi-dimensional plasticity formulations consisting of a yield surface, hardening law, and flow rule.

Many nonlinear codes use a hyperbolic equation to model the backbone curve (e.g., DEEPSOIL: [7]; D-MOD: [8]; and Tess: [9]). The hyperbolic formulation was first introduced by Kondner and Zelasko [10] and later modified by, for example, Hardin and Drnevich [11] and

Darendeli [12]. In the special case where the desired modulus reduction curve happens to be hyperbolic, then these models are capable of precisely matching the desired modulus reduction curve. However, the desired modulus reduction curve generally does not correspond to a hyperbolic backbone function, resulting in a misfit between the user-input modulus reduction curve and the hyperbolic curve.

Small misfits in the modulus reduction curve can translate to significant misfits in the stress-strain curve at high strain, resulting in errors in the desired shear strength (e.g. [4], [5], [6], [13]). To address this problem Hashash et al. [14] suggests that the high strain portion of the user-specified modulus reduction curve can be adjusted so that the resulting fitted curve provides the correct shear strength. However, this increases the misfit at low strain. Furthermore, Matasovic and Vucetic [8] introduced a modified version of the hyperbolic Kondner and Zelasko model where the introduction of two curve-fitting constants improves the modulus reduction curve match. Yee et al [15] proposed a hybrid procedure where the modulus reduction curve is modified to match the shear strength at high strains and obtain a more reasonable backbone curve. The procedure utilizes the prescribed modulus reduction curve below a transition strain, γ_t, and a hyperbolic model above γ_t. The stress and tangent modulus values are continuous at γ_t. However, the Yee et al. model cannot be perfectly fit by a hyperbolic model, often resulting in a mismatch between the desired shear strength and that achieved in the nonlinear site response code. Groholski et al. [16] proposed a new general quadratic hyperbolic (GQ/H) model in which the functional form of the backbone curve is derived from the bivariate quadratic equation. This quadratic equation is fitted to the modulus reduction curve at strains lower than a specified shear strain level. At large strains the quadratic equation is set to match a target shear strength. Between the small strain behavior and the shear strength the model provides flexibility in the nonlinear behavior. Although the GQ/H model constitutes a significant improvement over previous models, the resulting curve does not perfectly fit the target modulus reduction curve.

Plasticity models aim at reproducing the behavior of a material by using a set of constitutive laws. They are usually composed of a flow rule, a hardening law, and one or several yield or bounding surfaces. Multi-dimensional plasticity models typically incorporate nonlinear behavior using either multiple nested yield surfaces or bounding surface formulations. In multiple yield surface models (e.g. [17], [18]), the backbone curve is controlled by setting the plastic modulus associated with each yield surface. The resulting backbone curve is piecewise linear when a constant plastic modulus is assigned to each yield surface. The PressureDependMultiYield and PressureIndependMutliYield [18] material models implemented in OpenSees can be configured to match a user-specified modulus reduction curve. In bounding surface plasticity models, the plastic modulus is defined based on the distance in stress space between a current point and an “image” point on a bounding surface (e.g., [19], [20], [21]). The hardening function that controls the evolution of the plastic modulus may be adjusted to match a desired modulus reduction curve. For example, Boulanger and Ziotopoulou [21] adjusted the PM4Sand model to match the modulus reduction and damping curves for sand by EPRI [22]. However, the modulus-reduction curve is "hard coded" and is not an input to the PM4Sand model, though users could conceivably alter the modeling constants to fit any desired modulus reduction curve (a significant effort).

3 Damping Behavior of Existing Models

Soil damping can arise from hysteretic cyclic loading behavior of the soil skeleton, relative displacement between the solid and fluid phases, or other sources of energy loss. Damping is commonly divided into the “small-strain” region where the soil response is elastic, which is often modeled using numerical procedures such as Rayleigh damping, or the “large-strain” region, which is modeled by the unload-reload behavior of the stress-strain model. Masing [23] rules

and extended Masing rules (e.g., [24], [25], [26]) are most common in nonlinear site response codes [2].

The extended Masing rules are stated as follow:

1. The stress-strain curve follows the backbone curve during initial loading.
2. If a strain reversal happens at point (γ_{rev}; τ_{rev}), the unloading or reloading curve has a shape that is identical to the backbone curve enlarged by a factor n. In its original paper, Masing used n=2, it was later modified by Pyke [24], where n can deviate from 2, to provide a better match of the damping at higher strain.
3. If the unloading or reloading curve exceeds the maximum past strain and intersects the backbone curve, it follows the backbone curve until the next stress reversal.
4. If the unloading or reloading curve crosses an unloading or reloading curve from a previous cycle, it follows the curve of that previous cycle.

When Masing rules are used with n=2, the initial slope of the unloading or reloading curve is equal to the maximum shear modulus G_{max}, and the model shows no hardening or softening (i.e. loops are closed).

Masing rules tend to over predict damping at large strains [27], and do not provide hysteretic damping at small strains (i.e., in the range where G/G_{max} = 1). Several solutions have focused on modifying the second Masing rule to obtain reasonable hysteretic damping at high strains. The Cundall-Pyke hypothesis [24] evaluates n based on the shear strength. This formulation improves damping at high strain and creates some degradation. To match the damping curve, Darendeli introduced a damping reduction factor now used in several codes [12]. This formulation does not create degradation, and only acts on the area of the stress-strain loops. Based on Darendeli's work, Phillips and Hashash [27], introduced a damping reduction factor that provides a better fit of the curve at large strains.

Small-strain damping is commonly modeled using frequency-dependent Rayleigh damping, which introduces mass- and stiffness-proportional viscous damping terms to the equation of motion. Most nonlinear codes utilize the formulation by Rayleigh and Lindsay [28], which enables matching a desired damping value at either 2 frequencies (two-mode Rayleigh damping) or 4 frequencies (extended Rayleigh damping). At other frequencies, damping is either too low or too high, making the damping frequency-dependent in a manner that is inconsistent with laboratory results [29,30]. Phillips and Hashash [27] established, and implemented in DEEPSOIL, a frequency-independent viscous damping formulation, based on the work of Liu and Gorman [31]. TESS [9,24] uses an unload/reload rule to produce hysteretic damping at low strains. The procedure however can result in over prediction of damping at large strains [2].

An important consideration for NL methods is that the authors are not aware of any published models that permit exact simultaneous matching of any user-input modulus reduction and damping curve. Desired modulus reduction and damping curves often deviate from hyperbolic behavior, forcing users to choose to fit certain behaviors while accepting misfits in others [32]. The model formulation in the next section provides a precise fit to a discrete user-input modulus reduction and damping curve.

4 Formulation of the ARCS Model

4.1 Backbone Curve

During initial/virgin loading, a backbone curve is derived from the desired modulus reduction curve, and is fit with cubic splines (Fig. 1). Cubic spline interpolation is a mathematical method that has been extensively described in numerous textbooks (e.g. [33]). The cubic splines pass through all of the user-input data points, resulting in a smooth continuous modulus reduction

curve and stress-strain backbone curve. For comparison with the cubic spline fit, Fig. 1 also shows a hyperbolic fit performed using two different approaches. In the first approach, the hyperbola is fit by least squares regression to the G/G_{max} and $\log(\gamma)$ values. This fitting results in a misfit at high strain that causes an under-prediction of shear strength in this case. The second approach fits the hyperbola to the stress-strain data, which provides a better fit of shear strength, but significant misfit to the modulus reduction curve at small strains. The cubic spline method is more flexible than fitting a single hyperbola because the cubic spline interpolation passes through all of the data points, precisely fitting the user-input data.

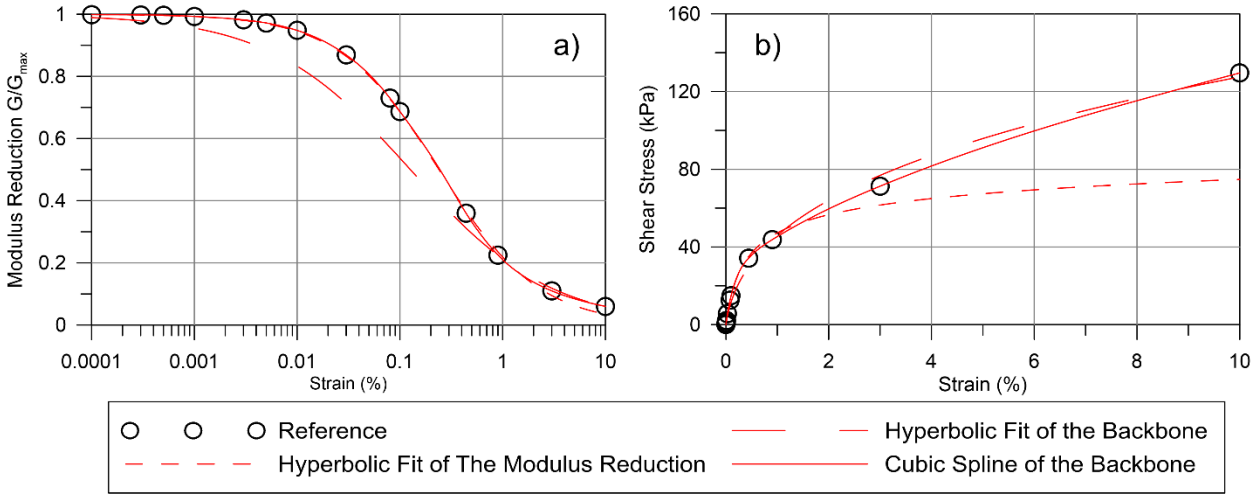

Figure 1 Evaluation of the curve fitting method on (a) the modulus reduction curve and (b) the backbone curve

4.2 Unload/Reload Rule

The unload-reload rule is formulated to satisfy the following criteria:

(i) The secant modulus of the stress-strain loops matches a user-defined modulus-reduction curve,

(ii) When subject to uniform cyclic strain amplitude input, the stress-strain loops close and repeat, exhibiting no cyclic degradation or stiffening,

(iii) The area inside the stress-strain loops matches a user-defined damping curve, even at small strains where the modulus-reduction value is one,

(iv) The stress-strain loops are concave about the secant modulus line.

4.2.1 Rotation of the Coordinate System

Upon the first unloading a coordinate transformation is introduced to control the modulus reduction and damping behavior. The values of strain and stress at the first unloading point are (γ_L, τ_L), and a target reversal point is defined as (γ_R, τ_R) = (-γ_L, -τ_L), as shown in Fig. 2. If unloading progresses, the curve will pass through the reversal point. A new coordinate system is defined such that the γ' axis lies along a line that runs through (γ_L, τ_L) and (γ_R, τ_R), at an angle θ from the γ axis, and the τ' axis is orthogonal to γ'. The origin of the rotated coordinate system, (γ_o,τ_o), lies at the center of (γ_L, τ_L) and (γ_R, τ_R), which happens to be (0,0) for the first unload cycle, but (γ_o,τ_o) may translate upon asymmetric loading, following rules described in the next section.

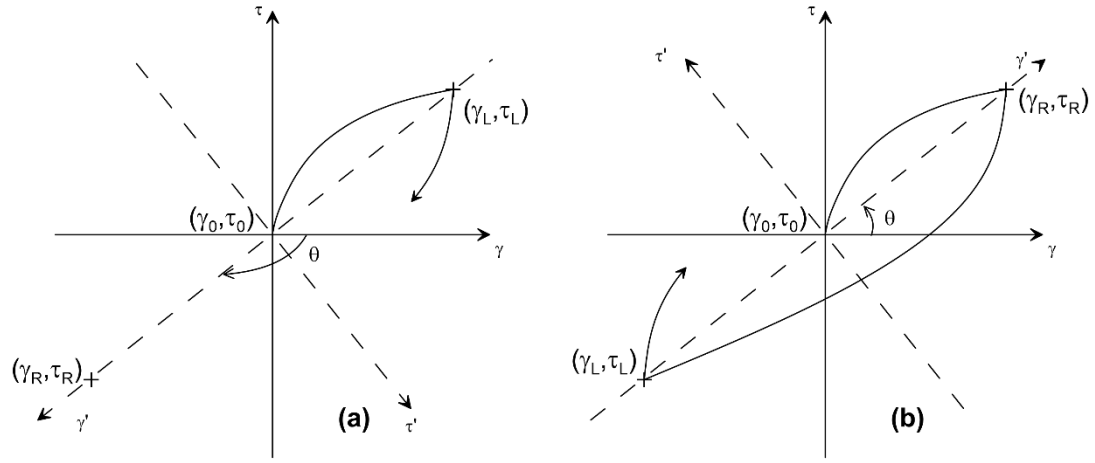

Figure 2: Stress-Strain loops during (a) Unloading and (b) Reloading

The definition of θ depends on the loading direction, defined by Eq. 1a for loading in the +γ direction and Eq. 1b for loading in the –γ direction.

$$\theta = \tan^{-1}\frac{\tau_R - \tau_L}{\gamma_R - \gamma_L} \tag{1a}$$

$$\theta = \tan^{-1}\frac{\tau_R - \tau_L}{\gamma_R - \gamma_L} - \pi \tag{1b}$$

The values in one coordinate system are related to those in another by Eqs. 2 and 3. Note that the units of γ' and τ' are meaningless because the coordinate transformation is performed on axes with differing units. However, this is inconsequential because the transformation is utilized merely as a means to satisfy the desired criteria, and an inverse transformation recovers the values of τ and γ.

$$\begin{pmatrix}\gamma\\ \tau\end{pmatrix} = \begin{pmatrix}\gamma'\cos\theta - \tau'\sin\theta + \gamma_0\\ \gamma'\sin\theta + \tau'\cos\theta + \tau_0\end{pmatrix} \tag{2}$$

$$\begin{pmatrix}\gamma'\\ \tau'\end{pmatrix} = \begin{pmatrix}(\gamma - \gamma_0)\cos\theta + (\tau - \tau_0)\sin\theta\\ -(\gamma - \gamma_0)\sin\theta + (\tau - \tau_0)\cos\theta\end{pmatrix} \tag{3}$$

To satisfy criterion (i), the value of θ must be selected to be compatible with a modulus reduction curve based on the cyclic shear strain amplitude. In this case, θ = atan(G_{sec}), and G_{sec} is interpolated from the modulus reduction curve at a cyclic strain amplitude, γ_c, defined as half of the peak-to-peak strain amplitude (Eq. 4).

$$\gamma_c = \frac{|\gamma_R - \gamma_L|}{2} \tag{4}$$

4.2.2 Stress-Strain Curve in Rotated Coordinate Space

Having defined the coordinate transformation, a function is now selected to define the unload-reload behavior in the transformed coordinate space. We select a biquadratic equation (Eq. 5)

because it is the simplest possible form that is symmetric about the τ' axis and contains three constants (a, b, and c) that can be solved to satisfy the three remaining criteria.

$$\tau' = a\,\gamma'^4 + b\,\gamma'^2 + c \tag{5}$$

The shape of the function describing a half loop in the transformed coordinate system is shown in Figure 3a, where the target reversal strain in the transformed system, γ'_{in}, is defined by Eq. 6. Note that the stress-strain loop is symmetric about the γ' and τ' axis in τ'-γ' space, but do not appear symmetric about the γ' axis in the τ-γ space. The lack of symmetry is due to stretching of the axes upon coordinate transformation due to the stress and strain axes having different units. The stress-strain curves in τ-γ space nevertheless exhibit a reasonable shape.

$$\gamma'_{in} = \frac{\gamma_R - \gamma_0}{cos\theta} \tag{6}$$

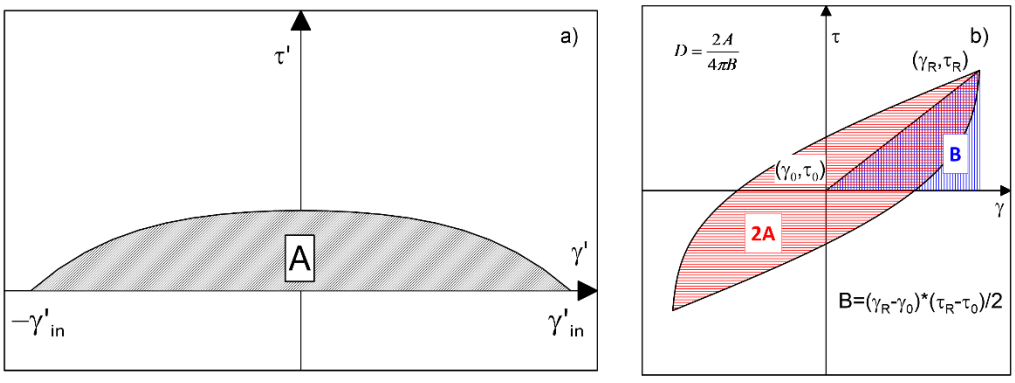

Figure 3 a) Half loop in the transformed coordinate system, and b) definition of damping

Criterion (ii), (iii), and (iv) are satisfied by Eqs. 7, 8, and 9, respectively.

$$\tau'(\gamma'_{in}) = 0 \tag{7}$$

$$\int_{-\gamma'_{in}}^{\gamma'_{in}} \tau'(\gamma')d\gamma' = A = \gamma'_{in} D\pi(\tau_R - \tau_0)cos\theta \quad (8)$$

$$\frac{d^2(\tau')}{d(\gamma')^2} \leq 0 \; for \; \gamma' \in -\gamma'_{in} .. \gamma'_{in} \quad (9)$$

Criterion (ii), requiring that the unload-reload loops close with no cyclic degradation or hardening, is satisfied by setting $\tau' = 0$ at $\gamma' = \pm\gamma'_{in}$ (Eq. 7). Criterion (iii), requiring the area inside the loop to match a target damping value, is satisfied by Eq. 8. The equivalent viscous damping ratio *D* is selected from the input damping ratio curve based on the cyclic strain amplitude (eq. 4). The damping ratio is defined by $D=2A/(4\pi B)$, where *A* is the area beneath half of the loop as shown in Fig. 3a, and *B* is the area of the triangle shown on Figure 3b and is equal to:

$$B = \frac{(\tau_R - \tau_0) * (\gamma_R - \gamma_0)}{2} \quad (10)$$

Criterion (iv), requiring that the stress-strain curve be concave about the secant shear modulus line is equivalent to requiring that $d^2(\tau')/d(\gamma')^2$ must be negative (Eq. 9). A bi-quadratic equation has two inflexion points that are symmetrical with respect to the apex. Forcing the inflexion points to lie at $\pm\gamma'_{in}$ automatically satisfies Eq. 9.

Substituting Eq. 5 into Eqs. 7, 8, and 9 and solving the linear system of equations for *a*, *b*, and *c* results in Eqs. 11, 12, and 13:

$$a = \frac{5\pi D cos\theta(\tau_R - \tau_0)}{32{\gamma'}_{in}^{4}} \tag{11}$$

$$b = -\frac{15\pi D cos\theta(\tau_R - \tau_0)}{16{\gamma'}_{in}^{2}} \tag{12}$$

$$c = \frac{25\pi D cos\theta(\tau_R - \tau_0)}{32} \tag{13}$$

Applying an inverse coordinate transformation to Eq. 5 using Eqs. 2 and 3 results in an implicit relationship between strain and stress (Eq. 14):

$$\tau = [(\gamma - \gamma_0)\cos\theta + (\tau - \tau_0)\sin\theta]\sin\theta + [a((\gamma - \gamma_0)\cos\theta + (\tau - \tau_0)\sin\theta)^4 + b((\gamma - \gamma_0)\cos\theta + (\tau - \tau_0)\sin\theta)^2 + c]\cos\theta + \tau_0 \tag{14}$$

In Eq. 14 the only unknown is τ, reducing the problem to a simple root-finding exercise. For the example problems presented herein, the root is solved using Ridders' Method [34], an algorithm based on the false position method which is unconditionally stable as long as the two initial guesses lie on each side of the root. The root is automatically bracketed when the initial guesses are set equal to the stress at the previous time step and the target stress point. Other methods converge more rapidly (e.g., Newton-Raphson), but are not always able to converge upon the desired root. Ridders' method converges more quickly than other unconditionally stable methods, such as the bisection method.

4.2.3 Asymmetrical Loading

Thus far, focus has been on symmetric loading, where (γ_R, τ_R) = (-γ_L, -τ_L), and (γ_o, τ_o) lies at (0,0). Asymmetrical loading conditions occur when (γ_R, τ_R) ≠ (-γ_L, -τ_L), meaning that the center of the unload-reload loop shifts away from the τ-γ origin, as illustrated in Fig. 4 and defined in Eq. 14.

$$\gamma_0 = \frac{\gamma_R + \gamma_L}{2} \tag{15a}$$

$$\tau_0 = \frac{\tau_R + \tau_L}{2} \tag{15b}$$

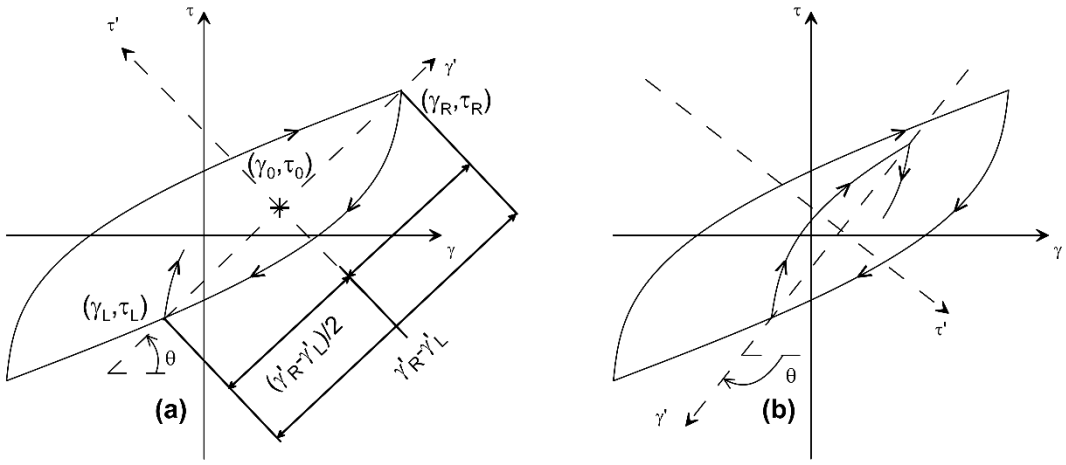

Figure 4 Asymmetrical Loading (a) Positive Loading (b) Negative Loading

Defining the values of γ_L and τ_L is straightforward; these values are simply the strain and stress at which the current reverse loading cycle began. Defining the values of γ_R and τ_R (i.e., the target value of strain and stress) involves three unload/reload rules, demonstrated through an example problem in Fig. 5. For brevity, the example problem is formulated in terms of strains (i.e., γ_L and γ_R), and the stress updating is omitted but follows the same logic. In Fig. 5a, monotonic loading progresses to the first reversal (Fig. 5a) at γ_1 and begins unloading such that $\gamma_L = \gamma_1$. The size of the unloading loop is not known at the onset of unloading, so the simplest assumption is that the target reversal point is $\gamma_R = -\gamma_1$. The first unload / reload rule is:

> *Rule 1: When an unloading cycle initiates from the monotonic backbone curve,* $\gamma_R = -\gamma_L$.

Having defined γ_R, the shape of the unload curve is defined by Eq. 14, and unloading progresses along this curve to a value γ_2 where a new reverse loading cycle begins. The value of γ_L is now updated to be equal to γ_2, while γ_R is updated to be equal to γ_1. The second unload / reload rule is:

> *Rule 2: When an unloading cycle initiates from a point that is not on the monotonic backbone curve, γ_L is updated to be the strain value at the start of the unloading cycle, and the previous value of γ_L becomes the current value of γ_R.*

Loading then progresses to a new unloading point at γ_3 (Fig. 5c) which is less than γ_1. At this point, $\gamma_L = \gamma_3$, and $\gamma_R = \gamma_2$ in accordance with Rule 2. Unloading then occurs to a new reloading point at γ_4 (Fig. 5d) where $\gamma_L = \gamma_4$ and $\gamma_R = \gamma_3$ in accordance with Rule 2. A reload cycle then loads beyond γ_3 (Fig. 5e) which brings us to the final unload / reload rule:

> *Rule 3: When a reloading cycle exceeds γ_R, the current values of γ_L and γ_R are erased as internal variables, and the previous values of γ_L and γ_R are reinstated.*

Rule 3 requires that all previous values of γ_L and γ_R must be stored in computer memory as internal variables until they are erased by a cycle that exceeds γ_R. In Fig. 5e, the loading cycle continues back to the monotonic backbone curve at γ_1, at which point $\gamma_L = \gamma_1$ and $\gamma_R = -\gamma_1$ in accordance with Rule 1, and all previous values of γ_L and γ_R are erased from computer memory.

Upon unloading and reloading, these rules can produce stresses lower than the backbone curve as illustrated in figure 5e. This departs from Masing rules, and is driven by the damping requirement.

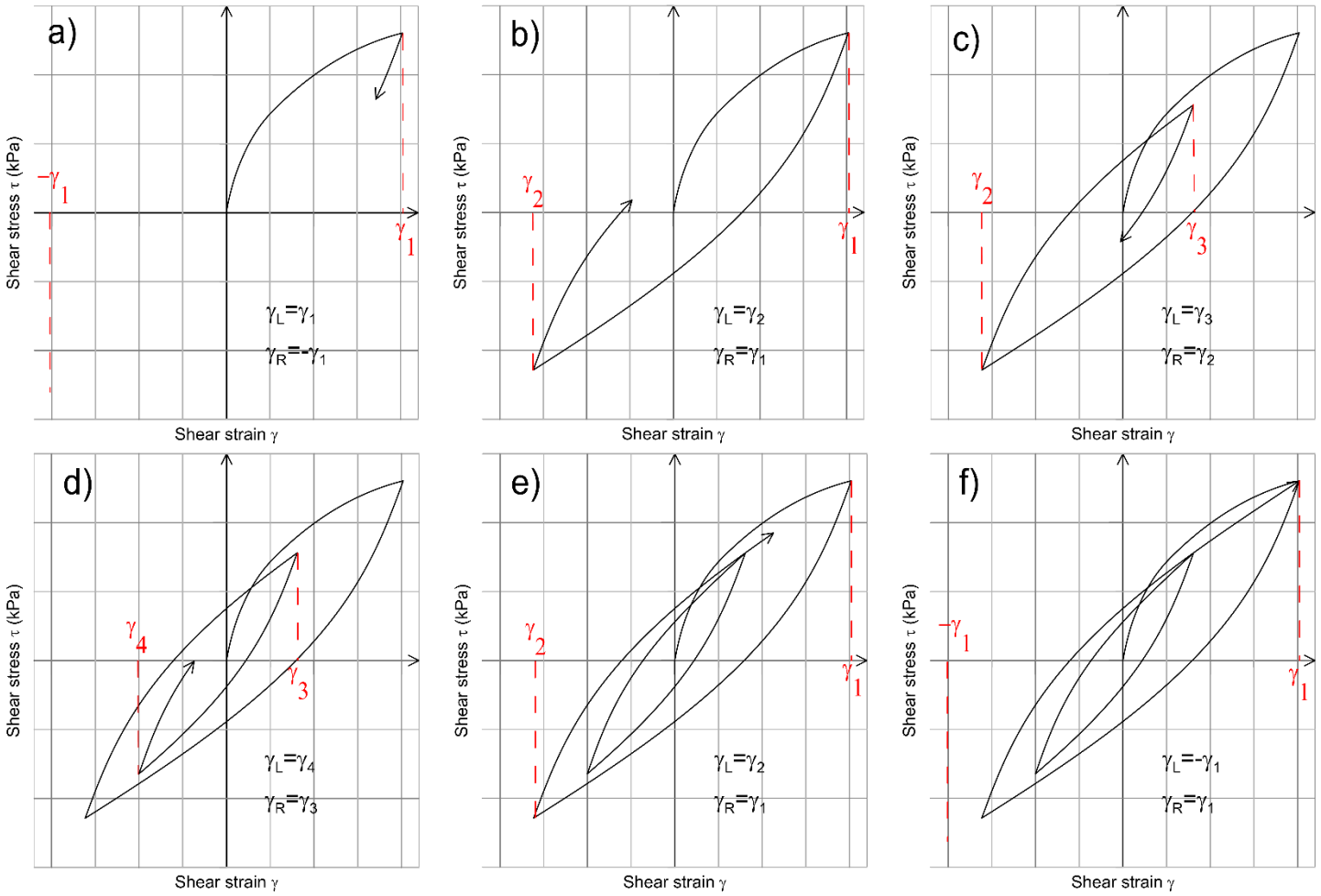

Figure 5 Evolution of the reversal strain vectors

5 Example Problems

An example problem is utilized to illustrate the following features of the model: (1) small-strain damping is explicitly modeled in the hysteretic formulation, (2) desired modulus reduction and damping curves can be perfectly matched, which differs from other commonly-used models, and (3) the solution does not depend on the size of strain increments utilized in a simulation. The target damping and modulus reduction curves for the example problem are calculated from Darendeli [12] for a soft clay with the following characteristics: *PI=40,* σ'_v*=47.5 kPa,* γ*=15 kN/m*^{3}*,* V_s*=80 m/s, OCR=1.15, and* K_0*=0.5*. The procedure presented by Yee et al. [15] was applied to

the computed modulus reduction curve to match a target undrained strength S_u = 17kPa and the transition strain was picked as γ_t = 0.03%. The target modulus reduction and damping curves are presented in Fig. 6. The modulus reduction curve is adjusted at high-strain to match a desired shear strength using the Yee et al. procedure, but the damping curve was simply extrapolated from Darendeli's functional form due to absence of recommendations for high-strain damping.

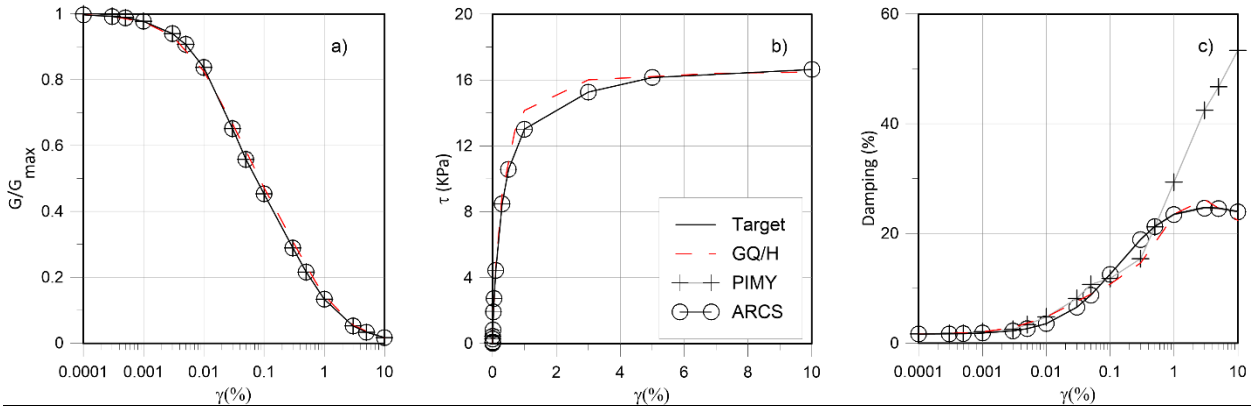

Figure 6. Modulus reduction (a), backbone (b) and damping ratio (c) curves predictions of different models for a clay PI=40, σ'$_v$=47.5 kPa, γ=15 kN, V_s=80 m/s, OCR=1.15 K_0=0.5.

5.1 Comparison with Existing Models

Figure 6 compares the ARCS model with two commonly used models: the GQ/H model used in DEEPSOIL 6.1 [16] and the PressureIndependMultiYield (PIMY) Model in OpenSees [18]. Response curves from the different models were back-calculated from the results of numerical simulations of a single element subjected to sinusoidal loading at different strain amplitudes, and comparisons with the desired modulus reduction and damping curves are presented in Figure 6. The proposed model and the PIMY both perfectly fit the target modulus reduction curve, while the GQ/H model results in a very slight misfit. The misfit appears very small when plotted as modulus reduction versus logarithm of shear strain, but is slightly more visible when plotted as a stress-strain curve. However, the GQ/H model is able to match the shear strength

which is one the input parameters of the model. Previous models using the hyperbolic model would have resulted in a potential mismatch of the target shear strength. The maximum strain level at which the model fits the modulus reduction curve was picked as the transition strain, and it was defined that 99% of the shear strength was reached at a strain of 10%.

Figure 6c compares the damping curves obtained with the different models. The proposed model explicitly includes small-strain hysteretic damping, whereas both the PIMY and GQ/H model (through the MRDF-UIUC fit) do not include small-strain hysteretic damping, relying instead on other formulations such as Rayleigh damping. OpenSees uses a two-point approach to Rayleigh damping (i.e., damping is specified at two frequencies, under-damping occurs between these frequencies, and over-damping occurs outside these frequencies). Frequency-dependent Rayleigh damping is not realistic, and care must be taken to ensure significant errors do not arise from this formulation. On figure 6c, the small strain damping indicated for the OpenSees simulation is the target damping. In reality the damping curve might be shifted up or down depending on the frequency of loading and whether the latter is lower higher than the specified two frequencies. DEEPSOIL implements a frequency-independent viscous damping formulation developed by Phillips and Hashash [27] which solves this problem, but is computationally demanding.

At large strains the PIMY model over predicts damping, which is a well-known aspect of Masing's rules [32]. The GQ/H model uses damping reduction factors at large strains, based on the formulation by Darendeli [12]. This results in a reasonable, but imperfect match of the damping curve, which over-predicted damping at some strain levels and under-predicted at others. The proposed coordinate transformation model perfectly matches the damping curve at all strain levels, eliminating the need for viscous damping, and avoiding over-damping at high strain. An outcome of including small-strain damping in the hysteretic formulation of the proposed model is that the initial unload-reload tangent modulus must be larger than the secant

shear modulus to accommodate non-zero area inside the stress-strain loop. This behavior is consistent with experimental observations (e.g. [35]).

5.2 Influence of Strain Increment

Many plasticity models utilize an explicit integration scheme that requires very small strain increments to achieve numerical stability, or an implicit integration scheme in which iterations are performed at each time step to ensure numerical stability. Both solutions are sensitive to the size of the strain increments in that different solutions will arise from different strain increment sizes because the tangent modulus for the increment is evaluated either the beginning (explicit) or end (implicit) of the increment. The algorithm presented herein is formulated differently in that the stress is computed as the physically meaningful root of Eq. 15 rather than by assuming a constant tangent modulus for a particular increment. The solution algorithm therefore does not depend on strain increment size, provided that the peak strain values are captured in the discretization (for accurate representation of the γ_L and γ_R internal variables). Figure 7 presents the prediction of the model for a sample of clay subject to sinusoidal loading at different strain levels using different discretization densities (4, 40, and 400 increments per cycle). Figure 7 shows that predictions for a cycle defined by 4 or 40 points lie exactly on the curves described by 400 points at every strain level. Thus the response of the model is independent of the amplitude of the strain increment.

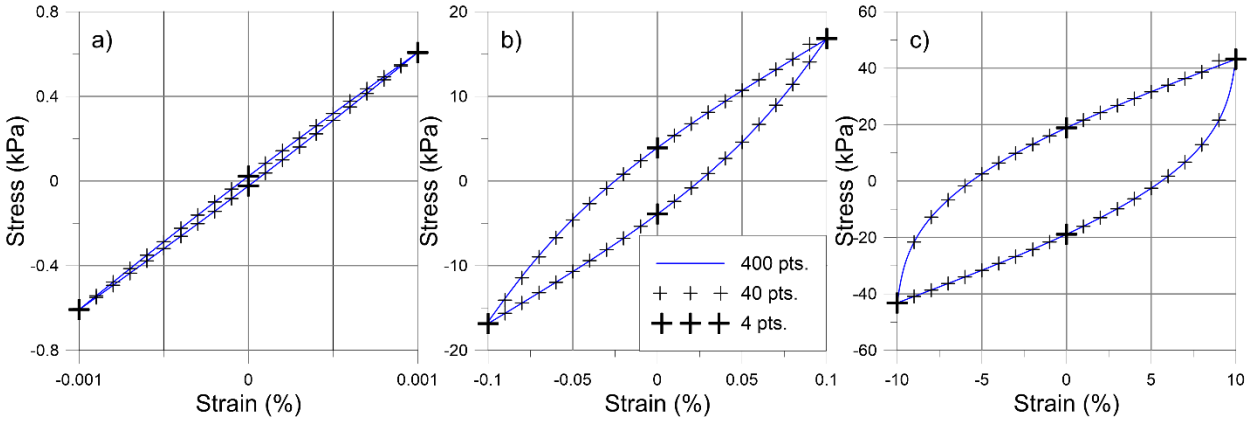

Figure 7 Comparison of the predictions of the model for cycles defined by 4, 40 and 400 points at strain level of (a) 0.001%, (b) 0.1%, (c) 10%.

6 Comparison with Direct Simple Shear Laboratory Tests

The University of California, Los Angeles (UCLA) bi-directional broadband direct simple shear device [36] was used to apply strain-controlled shear demands on Silica No. 2 dry sand and nearly saturated Sherman Island peat specimens with height and diameter of 25.4 and 72.6 mm respectively. The strain histories were deliberately irregular, involving local unloading and reloading cycles of small amplitudes. The peat was tested at higher strain amplitude than the sand because greater shear strains tend to develop in softer soils during earthquake loading. The results of the tests are compared with the predictions of the ARCS model, GQ/H in DEEPSOIL and the PressureIndependMultiYield (PIMY) model for the test on peat and the PressureDependMultiYield (PDMY) model for the test on sand in OpenSees.

6.1 Direct Simple Shear Tests

Silica No. 2 is a uniform sand with a median particle size D_{50}=*1.60 mm*, a coefficient of uniformity C_u=*1.29* [37] and maximum and minimum dry densities of 1.610 and 1.349 gr/cm^3, respectively. The dry pluviated specimen of Silica No.2 was prepared at a relative density of

42%, and then consolidated to a vertical pressure of 100kPa. The vertical pressure was kept constant during shear to obtained a drained loading condition. The loading path consisted of strain-controlled triangular functions in which three cycles of constant strain amplitude of 0.03% were followed by three cycles at 0.08%, and so on for 0.44% and 0.9%. An irregular loading path was then applied in which small unloading and reloading cycles were superposed on the 0.9% amplitude triangular function.

A peat specimen retrieved from a depth of 1.7 m from Sherman Island in the Sacramento-San Joaquin Delta, California was tested under undrained conditions using a similar irregular triangular loading path, but with shear strain amplitudes of 1.3%, 6.8%, and 13.6%. Details of the peat properties are provided by Shafiee [38]. The specimen was consolidated to σ_{vc}' = 60.4 kPa, and then unloaded to 31.3kPa to achieve an overconsolidation ratio (OCR) of 1.93. The organic content of the sample was 75%. The vertical stress was varied during shearing to maintain constant specimen height using a servohydraulic actuator and feedback control loop. Constant height testing achieves undrained loading conditions.

6.2 Model Input Parameters

The input modulus reduction curves were derived using the cyclic testing on the simple shear device supplemented by inferred shear modulus at strains lower than the device capabilities. The maximum shear modulus was calculated by dividing the shear modulus measured at the lowest strain level, by the G/G_{max} ratio calculated from the empirical relationship at the same strain level, to ensure the curves are continuous. The inferred maximum shear modulus for sand and peat was 23504 kPa and 877 kPa, respectively, which correspond to shear wave velocities of 128 m/s and 28 m/s. The inferred modulus values were then calculated by multiplying the normalized modulus reduction (G/G_{max}) calculated from Menq [39] and Kishida et al. [40], for

sand and peat respectively, by the maximum shear modulus. The modulus reduction curves obtained and the associated hyperbolic fits are plotted in Fig. 8.

The damping curves were derived by fitting cubic splines to the lab data and inferred points. For sand, the inferred points were calculated from Menq [39]. For peat, the lowest measured damping value (1.9%) was on the order of small-strain values from previous studies [40], and the inferred values were all taken as 1.9% (Fig. 8).

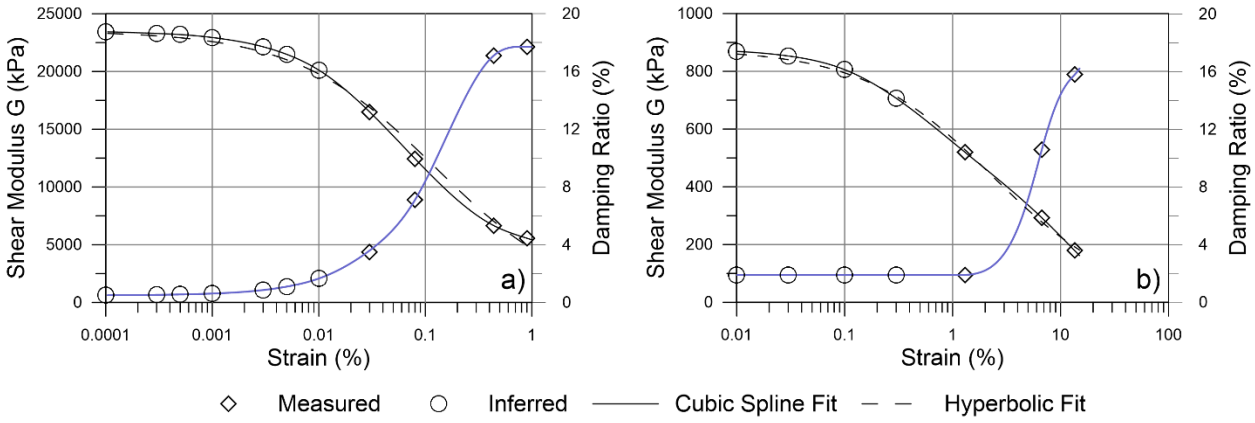

Figure 8 Input Modulus Reduction and Damping Curves a) Test on Sand b) Test on Peat

6.3 Simulations of Direct Simple Shear Tests

Figure 9 and 10 present the stress-strain loops measured in the lab and predicted by the present model (9a and 10a), DEEPSOIL using the GQ/H model (9b and 10b), and OpenSees (9c and 10c), for the tests on sand and peat respectively. For the test on sand, the PDMY model was used even though the predictions would not differ if the PIMY model was used since the sand was dry and tested under drained conditions, therefore inducing no change in confining pressure. During shearing the sand sample exhibits hardening, and the secant shear modulus increases with the number of cycles. This behavior of dry cohesionless soils has been reported previously by Silver and Seed [41], and is related to densification of the sand during cyclic loading. Our model does not predict hardening because it utilizes a single modulus reduction curve (and hence monotonic backbone curve), but the qualitative nature of the loops are in

close agreement with the test results. For both tests, the areas of the predicted stress strain loops agree with the damping curve, and plot very close to the test results. Furthermore, when a small unload-reload cycle moves back on to the monotonic backbone curve, a sharp change in slope is observed in both the test data and the model predictions.

The GQ/H model in DEEPSOIL slightly over-predicts the stresses during initial loading for the test on sand (figure 9b) and for the test on peat but accurately matches the shear strength. This over-prediction arises from the compromise that is taken when fitting the input modulus reduction curve and the target shear strength. Even though the GQ/H and the proposed ARCS model have the same target shear strength and modulus reduction curve, the stress-strain curves are different due to the different assumptions of the models. The unload/reload loops also follow different assumptions and therefore have different shapes. OpenSees follows the backbone curve, and is able to capture the initial loading of the soil properly for both the peat and sand (figure 9c and 10c). However, the OpenSees model under-damps the sand response and over-damps the peat response at high strain. Furthermore, the stress-strain behavior exhibits piecewise linear behavior due to the nature of the nested yield surfaces, whereas the laboratory data exhibits a smooth stress-strain curve.

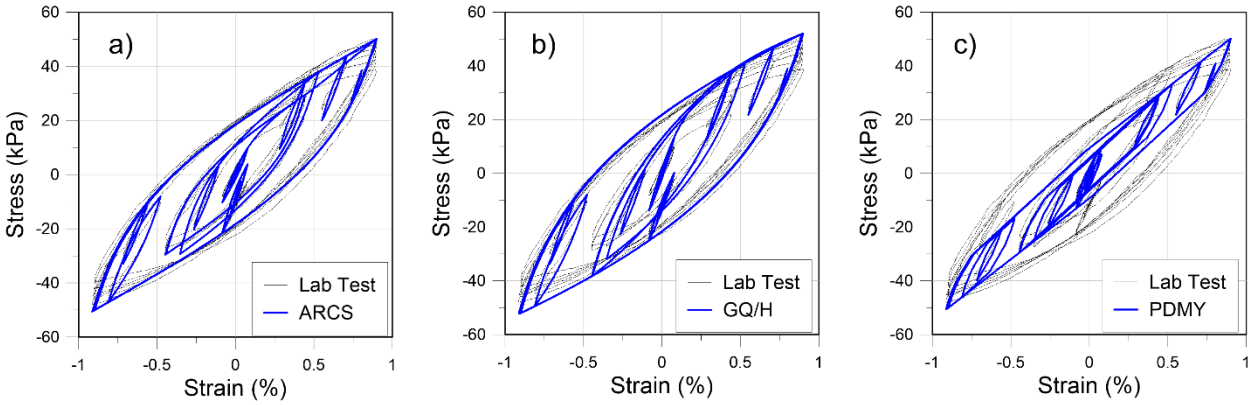

Figure 9 Stress-Strain loops measured in simple shear test on Silica No. 2 dry sand and predicted by: a) proposed model, b) GQ/H, c) PDMY in OpenSees

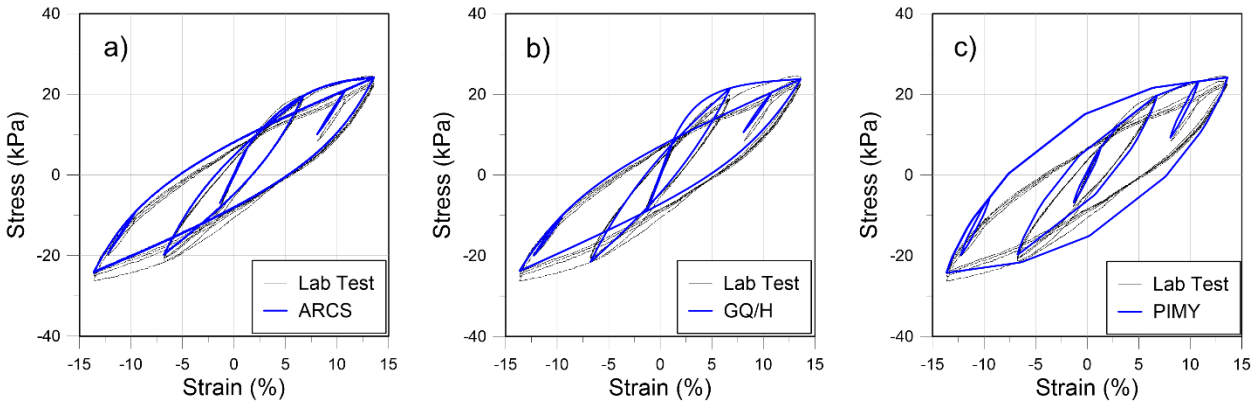

Figure 10 Stress-Strain loops measured in simple shear test on Sherman Island peat and predicted by: a) our model, b) GQ/H, c) PIMY in OpenSees

7 Nonlinear Ground Response Simulations

Ground response simulations performed in Deepsoil 6.1 are used to illustrate the performance of the model. The ARCS has been implemented in DEEPSOIL using the newly developed User-Defined Model feature. Two ground motions were applied to a 30m-profile of soft soil with PI=30. The two ground motions were sourced from the collection of motions of Baker et al. [42], which are intended to be ground motions representing rock conditions. From this ground motion records database, motion 8 and motion 23 were selected. Motion 8 is the north component of the motion (azimuth 0°) recorded at the Lamont 531 station during the Duzce earthquake, and has a peak horizontal acceleration of 0.16 g. Motion 23 is the east component of the motion (azimuth 90°) recorded at the WNT station during the Chi-Chi earthquake, and has a peak horizontal acceleration of 0.96 g. A constant unit weight was used (18 kN/m^3), and the profile was divided in 30 layers.

Modulus reduction and damping curves were calculated from Darendeli's equations [12] at every depth, and the modulus reduction curve was corrected for shear strength following the Yee et al. [15] procedure. The target shear strength was calculated using the SHANSEP

approach [43] based on the equation 16, with b=0.8 and $(s_u/\sigma'_{vc})_{NC}$=0.3. The shear strength, effective stress, preconsolidation pressure, and shear wave velocity profiles are presented in figure 11.

$$s_u = \sigma'_v \cdot OCR^b \cdot \left(\frac{s_u}{\sigma'_v}\right)_{NC} \tag{16}$$

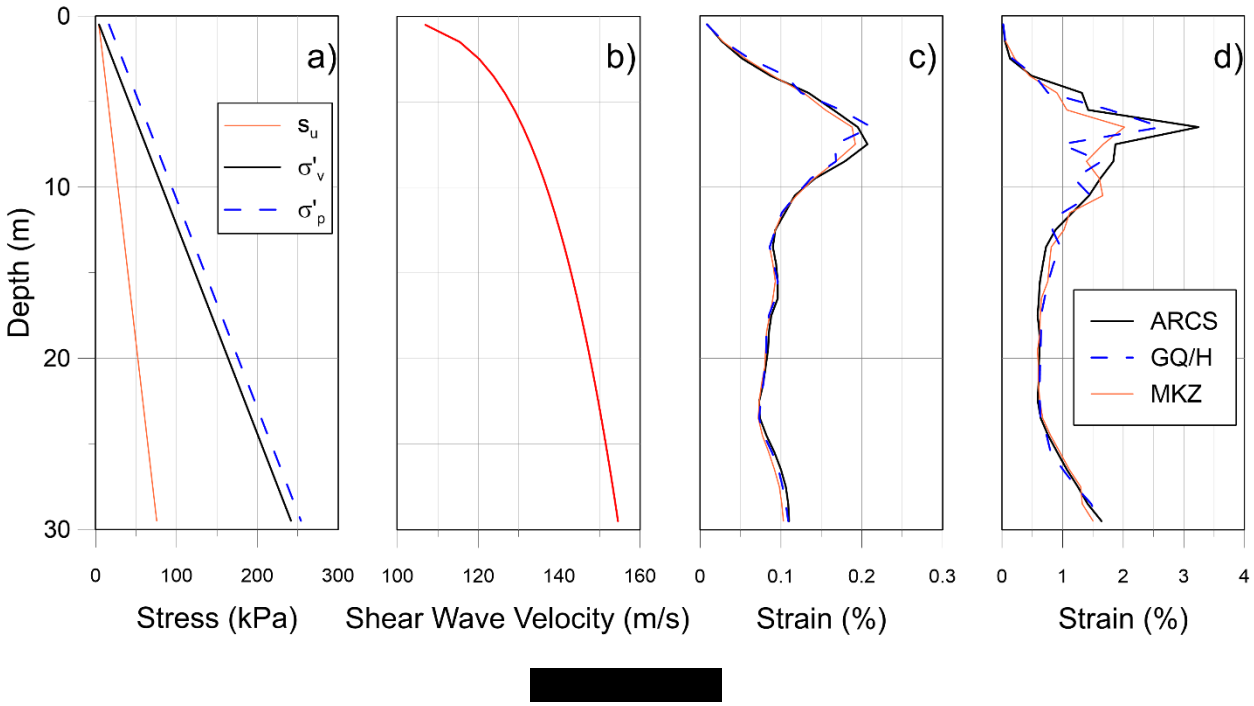

Figure 11 Effective stress (a), shear strength (a), OCR (b), and Shear wave velocity (b) profiles. Maximum mobilized shear strain profiles for the low (c) and large (d) amplitude motion.

The predictions of the model are compared with the predictions of the modified Kodner and Zelasko model (MKZ) using the same input curves, and the predictions of the GQ/H model using Darendeli's initial curves and the same target shear strength. Note that both the MKZ and the GQ/H models use the MRDF-UIUC unload/reload rules. As previously discussed the MKZ model is not set to match a target shear strength and induces a misfit of the modulus reduction curve which induces a misfit of the shear strength. On the contrary the GQ/H model matches a target shear strength and provides a smooth transition between an input modulus reduction

curve and the target shear strength. This transition is not fully based on the modulus reduction curve and in the present set of simulations, sometimes predicts an overly stiff response of the material. Both models induce a slight misfit of the input damping curve, especially at large strains. For both models the small strain damping is modeled using the frequency independent viscous damping formulation.

Figure 12 presents the response spectra for the surface motions and input motions for all the simulations. All models display a similar response, especially at longer periods. However, the PGA (S_a at high frequency) prediction by the MKZ model is lower than the other two models in both cases whereas the GQ/H model and the ARCS model predict similar PGA. For the larger motion there are some small differences in the response spectra even at long periods. However, the maximum mobilized shear strain profiles shown in Figure 11 c and d clearly illustrates the differences between the models. For the small motion, all models predict a similar maximum shear strain, but for the larger motion the MKZ model predicts a peak shear strain that is about half that of the ARCS model. This difference is explained by the misfit of the shear strength. In this example the MKZ constantly over-predict the target shear strength which results in an under-prediction of the mobilized shear strain. The difference between the GQ/H model and the ARCS model can be explained by the over-stiffness observed in the transition zone (between the target modulus reduction curve and the target shear strength), and by the slight over-prediction of the damping curve at large strains.

Computational times of all models were compared, and because the ARCS model does not use viscous damping, it ran about 2.5 times faster than the MKZ, and the GQ/H models, which had similar computational times. The reduction in run-time is attributed to the fact that the proposed model uses a hysteretic formulation for small-strain damping, whereas the other models use frequency independent viscous damping whose formulation is particularly computationally intense. When viscous damping is used, the damping matrix is being updated at every time step

which slows down significantly the computations. Other ground response simulations performed on more complex profiles showed a similar performance with, at times, even greater speed improvement.

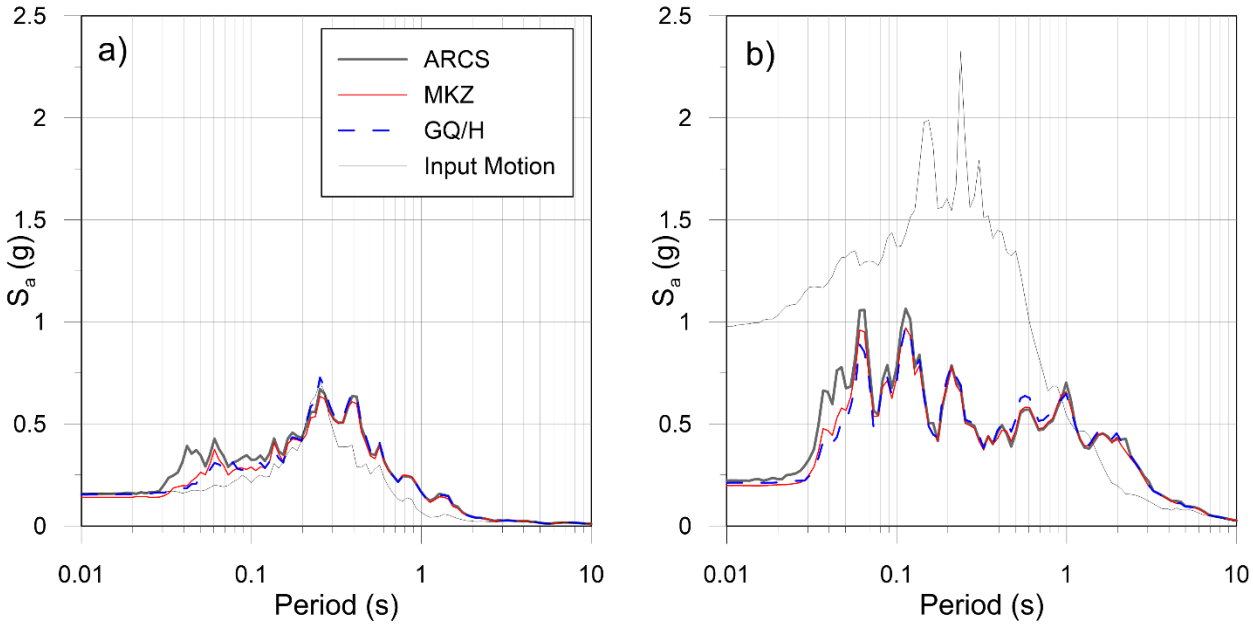

Figure 12 Response spectra for (a) small amplitude input motion (motion 8) (b) large amplitude input motion (motion 23)

High-frequency noise was observed in some of the simulations using the fully hysteretic damping scheme of the ARCS model. This unrealistic high frequency content has been observed by other researchers using different finite element and finite difference codes, and does not pertain specifically to DEEPSOIL. This noise is a known artifact of the Newmark integration algorithm [44], and arises because viscous damping was not used in the model formulation. The noise can effectively be removed by using an appropriate combination of viscous damping and hysteretic damping to achieve the desired overall damping ratio. Alternatively, integration algorithms have been proposed to solve this problem such as the α-

method [45] also known as the Hilber-Hughes-Taylor method. However, this integration algorithm is not currently available in DEEPSOIL,.

8 Conclusions

In this paper we presented a one dimensional nonlinear model for site response analysis called ARCS that departs from two concepts commonly used by site response models. Initial loading is not controlled by the widely used hyperbolic model, but instead uses a cubic spline fit of the backbone curve to match any modulus reduction curve. The hysteretic behavior of the soil is not controlled by the original or the extended Masing's rules, but is controlled by a new unloading and reloading rule that uses a coordinate transformation approach to calculate the shear stress, regardless of the amplitude of the strain increment. This unloading reloading rule easily controls the damping in the transformed coordinate system and provides a perfect fit of any damping curve.

The model captures small-strain hysteretic damping, thereby eliminating the need for Rayleigh damping, and it does not over-damp at high strain, which is a well-known problem associated with Masing's rules. The ARCS model is well suited for total stress 1D ground response analysis, and has been implemented in DEEPSOIL using the newly developed User-Defined model feature. The model proves to be faster than existing models because it does not require a viscous damping formulation for small-strain damping.

The one-dimensional kinematic hardening framework developed herein can potentially be implemented in a multi-dimensional plasticity formulation for more advanced numerical simulations. Such formulations could potentially capture the cyclic stiffening behavior exhibited by the sand as it densified during shearing, and the cyclic degradation behavior exhibited by the peat in constant volume shearing. However, such an implementation would require a method for

updating the backbone curve as the effective stress and/or void ratio changes during shear. Implementation and extension of the model is reserved for future publications.

Acknowledgments

The authors would like to thank Professor Jonathan P. Stewart and Youssef Hashash for their insightful comments, and for sharing with us their latest work on this topic. The authors also thank Michael Musgrove and Youssef Hashash for developing the user-defined model option in DEEPSOIL, and for their help with the implementation of the proposed model. Finally, the authors would like to thank the reviewer for the insightful comments, specifically about the observed unrealistic high-frequency response. This research was funded by the National Science Foundation under grant No. CMMI 1208170. Any opinions, findings, and conclusions or recommendations expressed in this material are those of the author(s) and do not necessarily reflect the views of the National Science Foundation.

References

[1] Kaklamanos, J., Bradley, B. A., Thompson, E. M., & Baise, L. G. (2013). Critical Parameters Affecting Bias and Variability in Site-Response Analyses Using KiK-net Downhole Array Data. *Bulletin of the Seismological Society of America*, 103(3), 1733-1749

[2] Stewart, J.P., Kwok, A.O., Hashash, Y.M.A., Matasovic, N., Pyke, R., Wang, Z., and Yang, Z. (2008). "Benchmarking of nonlinear geotechnical ground response analysis procedures," *Report PEER 2008/04*, pacific Earthquake Engineering Research Center, University of California, Berkeley.

[3] Kaklamanos, J., Baise, L. G., Thompson, E. M., & Dorfmann, L. (2015). Comparison of 1D linear, equivalent-linear, and nonlinear site response models at six KiK-net validation sites. *Soil Dynamics and Earthquake Engineering*, 69, 207-219.

[4] Groholski, D. R., Hashash, Y. M. A., Musgrove, M., Harmon, J., and Kim, B. (2015) " Evaluation of 1-D Non-linear Site Response Analysis using a General Quadratic/Hyperbolic Strength Controlled Constitutive Model" *6th International Conference on Earthquake Geotechnical Engineering, Christchurch, New Zealand*

[5] Afacan, K., Brandenberg, S., and Stewart, J. (2014). "Centrifuge Modeling Studies of Site Response in Soft Clay over Wide Strain Range." *J. Geotech. Geoenviron. Eng.*, 140(2), 04013003.

[6] Zalachoris, G., and E. M. Rathje (2015). Evaluation of one-dimensional site response techniques using borehole arrays, *J. Geotech. Geoenviron. Eng.*, Paper 04015053

[7] Hashash, Y.M.A. and D. Park (2001). "Non-linear one-dimensional seismic ground motion propagation in the Mississippi embayment," *Eng. Geology*, Amsterdam, 62(1–3), 185–206.

[8] Matasovic, N. and M. Vucetic (1993). "Cyclic Characterization of Liquefiable Sands," *J. of Geotech. Eng.*, ASCE, 119(11), 1805-1822

[9] Pyke, R.M. (2000). *TESS: A computer program for nonlinear ground response analyses*. TAGA Engineering Systems & Software, Lafayette, Calif.

[10] Kondner, R. L., and J.S. Zelasko (1963). "A hyperbolic stress-strain formulation of sands," *Proc. of 2nd Pan American Conference on Soil Mechanics and Foundation Engineering,* Sao Paulo, Brasil, 289–324

[11] Hardin, B.O. and V.P. Drnevich (1972). “Shear modulus and damping in soils: design equations and curves,” J. of the Soil Mechanics and Foundations Div., ASCE, 98 (SM7), 667–692

[12] Darendeli, M. (2001). “Development of a new family of normalized modulus reduction and material damping curves.” *Ph.D. Thesis*, Dept. of Civil Eng., Univ. of Texas, Austin.

[13] Chiu, P., D.E. Pradel, A.O.L. Kwok and J.P. Stewart (2008). “Seismic response analyses for the Silicon Valley Rapid Transit Project,” *Proc. 4th Decennial Geotechnical Earthquake Engineering and Soil Dynamics Conference*, ASCE, Sacramento, CA

[14] Hashash Y. M. A., Phillips C., and Groholski D. R. (2010) “Recent advances in non-linear site response analysis.” *Fifth International Conference on Recent Advances in Geotechnical Earthquake Engineering and Soil Dynamics, San Diego 2010.*

[15] Yee E., Stewart J.P., Tokimatsu K. (2013) “Elastic and large-strain nonlinear seismic site response from analysis of vertical array recordings”, *J. Geotech. Geoenvion. Eng.,* 139 (10), 1789-1801.

[16] Groholski, D. R., Hashash, Y. M., Kim, B., Musgrove, M., Harmon, J., & Stewart, J. P. (2016). “Simplified model for small-strain nonlinearity and strength in 1D seismic site response analysis.” *Journal of Geotechnical and Geoenvironmental Engineering*, 142(9), 04016042.

[17] Prevost, J.H. (1985). “A simple plasticity theory for frictional cohesionless soils,” *Soil Dyn. Earthquake Eng.*, 4(1), 9-17

[18] Elgamal A, Yang Z, Parra E, Ragheb (2003) “A Modeling of cyclic mobility in saturated cohesionless soils.” *Int J Plasticity*, 19:883-905.

[19] Assimaki, D., Kausel, E., and Whittle, A. J. (2000). "Model for dynamic shear modulus and damping for granular soils." *J. Geotech. Geoenvion. Eng.,* 126(10), 859-869.

[20] Dafalias, Y. F., & Manzari, M. T. (2004). “Simple plasticity sand model accounting for fabric change effects.” *Journal of Engineering mechanics*, 130(6), 622-634.

[21] Boulanger, R. W., Ziotopoulou K. (2015). "PM4SAND (Version 3): A sand plasticity model for earthquake engineering applications." *Report No. UCD/CGM-15-01*, Center for Geotechnical Modeling, Department of Civil and Environmental Engineering, University of California, Davis, CA, 108 pp.

[22] Electrical Power Research Institute, EPRI (1993). “Guidelines for determining design basis ground motions,” *Rpt. No. EPRI TR-102293*, Electrical Power Research Institute, Palo Alto, CA.

[23] Masing, G. (1926). “Eigenspannungen and verfertigung beim messing.” *Proc. 2nd Int. Congress on Applied Mech.*, Zurich, Switzerland

[24] Pyke, R.M. (1979). “Nonlinear soil models for irregular cyclic loadings,” *J. Geotech. Eng.*, ASCE, 105(GT6), 715-726.

[25] Wang, Z.L., Y.F. Dafalias, C.K. Shen (1990). “Bounding surface hypoplasticity model for sand,” *J. Eng. Mech.,* ASCE, 116 (5)

[26] Vucetic, M. (1990). “Normalized behavior of clay under irregular cyclic loading.” *Canadian Geotech. J.*, 27, 29-46.

[27] Phillips C., and Hashash Y. M. A. (2009) “Damping formulation for nonlinear 1D site response analyses.” *Soil Dynamics and Earthquake Engineering*, 29(7), 1143-1158.

[28] Rayleigh, J.W.S and R.B. Lindsay (1945). *The theory of sound, Dover Publications*, New York

[29] Lai, C.G., Rix, G.J., (1998). “Simultaneous inversion of Rayleigh phase velocity and attenuation for near-surface site characterization.” *Report No. GIT-CEE/GEO-98-2*. Georgia Institute of Technology, School of Civil and Environmental Engineering

[30] Vucetic, M., G. Lanzo, and M. Doroudian (1998). “Damping at small strains in cyclic simple shear test.” *J. Geotech. and Geoenviron. Eng.*, ASCE, 124(7), 585-594.

[31] Liu, M., and Gorman, D. G. (1995). "Formulation of Rayleigh damping and its extensions." *Computers and Structures*, 57(2), 277-285.

[32] Kwok, O.L.A., J.P. Stewart, Y.M.A. Hashash, N. Matasovic, R.M. Pyke, Z.L. Wang, and Z. Yang (2007). “Use of exact solutions of wave propagation problems to guide implementation of nonlinear seismic ground response analysis procedures,” *J. of Geotech. & Geoenviron. Eng.*, ASCE, 133, no. 11, 1385–1398

[33] De Boor, Carl. "A Practical Guide to Splines" Springer-Verlag, New York 1978

[34] Ridders C. J. F. (1979) “A New Algorithm for Computing a Single Root of a Real Continuous Function.” IEEE Transactions on circuits and systems, 979-980.

[35] Doroudian, M. and Vucetic, M., (1995). “A Direct Simple Shear Device for Measuring Small-Strain Behavior,” *ASTM Geotechnical Testing Journal*, Vol. 18. No. 1, pp. 69-85.

[36] Duku, PM, JP Stewart, DH Whang, and R Venugopal (2007). “Digitally controlled simple shear apparatus for dynamic soil testing,” *Geotech. Testing Journal*, ASTM, 30 (5), 368-377.

[37] Duku, PM, JP Stewart, DH Whang, and E Yee, (2008). “Volumetric strains of clean sands subject to cyclic loads,” *J. Geotech. & Geoenv. Engrg.*, ASCE, 134 (8), 1073-1085.

[38] Shafiee A. (2015) “Cyclic and Post-Cyclic Behavior of Sherman Island Peat”, *Ph.D. Dissertation*, University of California, Los Angeles, CA, USA.

[39] Menq F.Y. (2003) “Dynamic properties of sandy and gravelly soils”, *Ph.D. Dissertation*, University of Texas at Austin, TX, USA, 364.

[40] Kishida, T. Boulanger, R., Abrahamson, N., Wehling, T., and Driller, M. (2009). “Regression Models for Dynamic Properties of Highly Organic Soils.” *J. Geotech. Geoenviron. Eng.*, 135(4), 533-543

[41] Silver, M. L., and Seed, H. B. (1971). "Volume changes in sands during cyclic loading." *Journal of Soil Mechanics and Foundation Division, American Society of Civil Engineers*, 97(SM9), 1174-1178

[42] Baker, JW, Lin, T., Shahi, SK, and Jayaram, N. (2011). “New ground motion selection procedures and selected motions for the PEER Transportation Research Program.” *PEER Technical Report 2011/03*. 106p.

[43] Ladd, C. C. and Foott, R. (1974), "New Design Procedure for Stability of Soft Clays", *Journal of Geotechnical Engineering*, 100 (GT7), pp. 763–786

[44] Hughes T. J. R. “Finite Element Method - Linear Static and Dynamic Finite Element Analysis.” Prentice-Hall, Englewood Cliffs, New Jersey, 1987.

[45] Hilber, H. M., Hughes, T. J., & Taylor, R. L. (1977). “Improved numerical dissipation for time integration algorithms in structural dynamics.” *Earthquake Engineering & Structural Dynamics*, 5(3), 283-292.